Nghiên cứu cơ chế và động học phản ứng giữa methylene blue với gốc tự do OH trong pha khí bằng phương pháp tính toán DFT

TÓM TẮT

Methylene blue (**MB**) là một loại thuốc nhuộm dị vòng thơm phổ biến, được sử dụng rộng rãi trong công nghiệp, đặc biệt là trong nhuộm giấy, bông, len, lụa và các loại sợi dệt khác. Cơ chế và động học liên quan đến quá trình phân hủy **MB** bởi gốc tự do $HO^{\bullet}$ trong pha khí đã được tính toán trong nghiên cứu này bằng phương pháp hóa học lượng tử. Trong pha khí, **MB** chủ yếu bị phân hủy thông qua cơ chế cộng gốc tự do vào nối đôi, trong đó gốc $HO^{\bullet}$ tấn công tại vị trí C4 ở nhiệt độ 298,15 K. Hằng số tốc độ tổng thể của bước 1 và bước 2 lần lượt là $3{,}24\times10^{10}$ $M^{-1}\ s^{-1}$ và $1{,}48\times10^{12}$ $M^{-1}\ s^{-1}$; quá trình này tạo ra ba sản phẩm chính. Hằng số tốc độ tổng thể của phản ứng phân hủy **MB** có xu hướng giảm dần trong khoảng nhiệt độ từ 253 đến 323 K.

Từ khóa: *methylene blue; tính toán DFT; oxidation; cơ chế; phân hủy.*

DFT Study on the mechanism and kinetics of the gas-phase reaction between methylene blue and OH radicals

ABSTRACT

Methylene blue (**MB**) is a common aromatic heterocyclic dye used in industry, especially for dying paper, cotton, wool, silk, and other textiles. The mechanisms and kinetics associated with the degradation of **MB** by the HO• radical in the gas phase were calculated in this study using quantum chemical calculations. In the gas phase, **MB** is predominantly degraded through a radical adduct formation mechanism that involves the HO• radical at the C4 position at a temperature of 298.15 K. The overall rate constants for steps 1 and 2 are 3.24×10^{10} M^{-1} s^{-1} and 1.48×10^{12} M^{-1} s^{-1}, respectively, and this process produces three principal products. The overall rate constant for **MB** degradation gradually decreases within the temperature range of 253 - 323 K.

Keyworks: *methylene blue; DFT study; oxidation; mechanism; chemical fate.*

1. INTRODUCTION

Methylene blue (**MB**, Figure 1) is an aromatic heterocyclic dye widely utilized in industry, particularly for dyeing silk, cotton, wool, paper, and other materials.[1-3] **MB** is a cationic dye that is resistant to natural degradation, posing a risk to ecological systems and potentially leading to different health problems for humans in the event of uncontrolled release, despite its recognized clinical use.[2,3] Our recent analysis revealed that, in water, **MB** exhibited a quick reaction with the HO• radical, characterized by an overall rate constant ranging from 5.51×10^9 to 2.38×10^{10} M^{-1} s^{-1}, and a lifetime of 11.66 hours to 5.76 years at temperatures between 273 and 383 K.[4] Nonetheless, the atmospheric degradation of **MB** has yet to be investigated. This study examines the thermodynamic and kinetic aspects of the reaction between **MB** and hydroxyl radicals in the gas phase through computational methods.

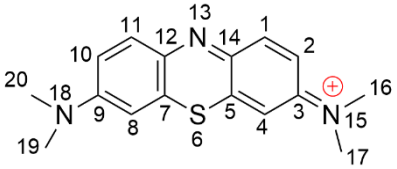

Figure 1. Structure of **MB**.

2. COMPUTATIONAL METHODS

Computational calculations for this investigation were performed using the Gaussian 16 software suite at the M06-2X/6-311++G(d,p) level of theory.[5] This methodology is widely recognized for its precision in determining thermodynamic and kinetic properties in modern computational chemistry studies.[6-8] Kinetic evaluations were conducted using the Quantum Mechanics-based Overall Free Radical Scavenging Activity (QM-ORSA) approach.[8-10] Under standard conditions of 1 M concentration and temperatures ranging from 253 to 323 K in the gas phase, the reaction rate constant (k) was computed employing Equation (1) and transition state theory (TST).[11-17]

$$k = \sigma\kappa \frac{k_B T}{h} e^{-(\Delta G^{\neq})/RT} \quad (1)$$

The Gibbs free energy of activation, denoted as $\Delta G^{\ddagger}$, is used in conjunction with the Boltzmann constant (k_B) and the Planck constant (h). Tunneling corrections (κ) were calculated based on the Eckart barrier model.[18] The reaction symmetry number is represented by σ. [19,20]

The radical adduct formation (RAF), or formal hydrogen transfer (FHT) pathways detailed in equations (2-3) can provide the mechanistic underpinning of the reaction between **MB** and HO•, with consideration to the molecular structure:[8,9,16]

RAF: MB-H + HO• → [HO-MB-H]• (2)

FHT: MB-H + HO• → MB• + H_2O (3)

3. RESULTS AND DISCUSSION

3.1. Topology optimization of MB

MB can exist in various conformers, the conformer with the lowest electronic energy was incorporated into the study. Topology optimization helps to clarify the molecular structure and determine the most stable conformer. This study employs the M06-2X/6-311++G(d,p) method to investigate optimized structure, the thermodynamic and kinetic properties of the degradation of **MB** by HO• radicals hydroxyl. The result of topology optimization of **MB** is presented in **Table 1**.

Table 1. Bond lengths (Å) and bond angles (°) in **MB**

Bond	Length	Bond	Length	Bond	Angle
C5–S	1.735	C7–S	1.735	C5–S–C7	103.4
C12–N13	1.328	C14–N13	1.328	C12–N13–C14	123.8
C3–N15	1.342	C2–C3	1.439	C2–C3–N15	120.6
C16–N15	1.462	C17–N15	1.460	C16–N15–C17	119.0
C9–N18	1.342	C9–C10	1,439	C10–C9–N18	120,6
C1–C2	1.356	C2–C3	1.439	C1–C2–C3	120.6
C3–C4	1.417	C4–C5	1.379	C3–C4–C5	120.6
C5–C14	1.434	C4–C5	1.379	C4–C5–C14	121.4
C5–C14	1.434	C1–C14	1.429	C1–C14–C5	117.0
C10–C11	1.356	C11–C12	1.430	C10–C11–C12	122.1
C11–C12	1.430	C12–C7	1.434	C11–C12–C7	121.4
C7–C8	1.379	C8–C9	1.417	C7–C8–C9	120.6

Table 1 illustrates that the C5–S bond length is equal to the C7–S bond length (1.735 Å), and these atoms form a bond angle of 103.4º. The C12–N13 bond length and C14–N13 are also equal, measured at 1.328 Å, with a corresponding bond angle of 123.8º. The bond lengths of C1–C2 (1.356 Å) and C4–C5 (1.379 Å) are shorter than those of C2–C3 (1.439 Å), C3–C4 (1.417 Å), and C5–C14 (1.434 Å). The bond angles C1–C2–C3 and C3–C4–C5 show only negligible differences (120.643º and 120.613º, respectively). Compared with the experimental crystal structure of **MB**,[21] the calculated bond lengths and bond angles exhibit no significant deviations. Therefore, the optimized structure of **MB** is in good agreement with the experimental structure and is thus suitable for subsequent computational analyses.

3.2. The reaction of MB with HO• in the atmospheric environment

3.2.1. Thermodynamic evaluation

To obtain initial insights into the reaction between **MB** and HO•, the degradation of **MB** in the gas phase was investigated by calculating the thermodynamic and kinetic parameters using the M06-2X/6-311++G(d,p) method at 298.15 K.

To assess the reactivity of **MB** at various carbon and nitrogen atomic sites via different reaction mechanisms, the Gibbs free energy change (ΔG°, kcal/mol) was evaluated. The computed values are summarized in **Table 2**. A positive ΔG° indicates a thermodynamically unfavorable reaction, which is non-spontaneous. As shown in **Table 2**, negative ΔGº values reflect thermodynamically favorable and spontaneous reactions. Based on the results, the **FHT** and **RAF** mechanisms are both spontaneous. Specifically, for the **RAF** mechanism, the ΔG° values at C1, C2, C3, C4, C5, N13, and C14 positions are all negative. Similarly, the **FHT**

mechanism exhibits negative ΔG^0 values at the C16 and C17 positions. The ΔG^0 values for these reactive sites range from −4.4 to −30.1 kcal/mol, indicating favorable thermodynamic conditions for these pathways. Therefore, the subsequent kinetic study will evaluate the thermodynamically favorable reactions ($\Delta G^o < 0$) proceeding via the **FHT** and **RAF** mechanisms.

Table 2. Gibbs free energy chnange (ΔG^o, kcal/mol) of the reaction between **MB** and HO$^\bullet$ via different mechanisms in the gas phase at 298.15 K

Mechanism	Position	ΔG^o
FHT	C16–H	−30.0
	C17–H	−30.1
RAF	N13	−11.1
	C1	−15.4
	C2	−17.9
	C3	−4.4
	C4	−16.1
	C5	−11.7
	C14	−11.6

3.2.2. Kinetic evaluation

The kinetic study of the degradation reaction of **MB** by HO$^\bullet$ in the gas phase was carried out using the M06-2X/6-311++G(d,p) method. The kinetic results are summarized in **Table 3** and the representative transition state structures are illustrated in **Figure 2**.

Table 3. Computed $\Delta G^{\neq}$ (kcal/mol), κ, rate constants (k_{Eck}, k_r, $k_{overall}$ M^{-1} s^{-1} (M^{-1} s^{-1}), and Γ (%) at 298.15 K, in the HO$^\bullet$ + **MB** in gas phase

Comp.	Mechanism	Position	$\Delta G^{\neq}$	κ	k_{Eck}	*r*	k_r	Γ	Product
MB	**FHT**	C16	6.0	2.0	1.51×10^{9}			**4.6**	**GI16**
		C17	5.5	1.9	3.01×10^{9}			**9.3**	**GI17**
	RAF	C1	10.1	1.4	7.23×10^{9}			0.0	
		C2	5.5	1.2	1.39×10^{9}			**4.3**	**GI2**
		C3	10.9	1.2	1.45×10^{5}			0.0	
		C4	3.7	1.1	2.65×10^{10}			**81.7**	**GI4**
		C5	12.7	1.3	7.83×10^{3}			0.0	
		N13	13.1	1.6	4.94×10^{3}			0.0	
		C14	8.2	1.3	1.51×10^{7}			0.0	
	***k*$_{overall}$ (MB** + HO$^\bullet$, step 1)				**3.24×10^{10}**			**100.0**	
GI4	**FHT**	C16	7.1	6.8	8.43×10^{8}	0.817	6.89×10^{8}	0.0	
		C17	9.5	2.5	5.24×10^{6}	0.817	4.28×10^{6}	0.0	
		C19	6.0	1.7	1.26×10^{9}	0.817	1.03×10^{9}	0.1	

Comp.	Mechanism	Position	$\Delta G^{\neq}$	κ	k_{Eck}	*r*	k_r	Γ	Product
		C20	6.2	1.8	$9.64x10^{8}$	0.817	$7.87x10^{8}$	0.1	
	RAF	C1	8.2	1.3	$7.83x10^{6}$	0.817	$6.40x10^{6}$	0.0	
		C2	1.6	1.1	$4.76x10^{11}$	0.817	$3.89x10^{11}$	**26.3**	**GP1**
		C3	3.8	1.2	$1.26x10^{10}$	0.817	$1.03x10^{10}$	0.7	
		C4			0.00	0.817	0.00	0.0	
		C5	6.9	1.5	$8.43x10^{7}$	0.817	$6.89x10^{7}$	0.0	
		C7	11.9	1.3	$1.63x10^{4}$	0.817	$1.33x10^{4}$	0.0	
		C8	2.6	1.1	$8.43x10^{10}$	0.817	$6.89x10^{10}$	**4.7**	**GP2**
		C9	13.5	1.2	$1.02x10^{3}$	0.817	$8.37x10^{2}$	0.0	
		C10	7.7	1.3	$1.69x10^{7}$	0.817	$1.38x10^{7}$	0.0	
		C11	10.9	1.3	7.8310^{4}	0.817	$6.40x10^{4}$	0.0	
		C12	11.8	1.4	$1.93x10^{4}$	0.817	$1.57x10^{4}$	0.0	
		C14	1.0	1.0	$1.20x10^{12}$	0.817	$9.84x10^{11}$	**66.5**	**GP3**
		N13	15.0	1.7	$1.08x10^{2}$	0.817	88.60	0.0	
	$k_{overall}$ (r) (**GI4** + HO•)						1.45 $x10^{12}$	**98.3**	
$k_{overall}$ (*r*) (**MB** + HO•, step 2)							**$1.48x10^{12}$**		

Based on the results presented in **Table 3**, the interaction between **MB** and HO• in the gas phase occurs rapidly, with an overall rate constant in the first step of 3.24×10^{10} $M^{-1}s^{-1}$. **MB** undergoes degradation via the **FHT** mechanism at the C16 and C17 positions, and the **RAF** mechanism at the C2 and C4 positions.

These computational results suggest that the first step reaction preferentially proceeds via the **RAF** mechanism, rather than through the **FHT** mechanism. The transition state originating from C4 contributes most significantly (81.7%) compared to the other three positions. This dominance can be attributed to the higher electron density at C4 relative to C2, making C4 more favorable for HO• radical addition. Within the **FHT** pathway, the reaction is more favorable at C17 (9.3%) than at C16 (4.6%), likely due to the lower bond dissociation energy of the C17–H bond compared to C16–H.

The reaction rate constants at these positions decrease in the following order: C4 (2.65×10^{10} M^{-1} s^{-1}) > C17 (3.01×10^{9} M^{-1} s^{-1}) > C16 (1.51×10^{9} M^{-1} s^{-1}) > C2 (1.39×10^{9} M^{-1} s^{-1}). Correspondingly, the transition state contributions decrease as follows: **GI4** (81.7%) > **GI17** (9.3%) > **GI16** (4.6%) > **GI2** (4.3%).

In the second step, reactions involving transition states **GI2, GI4, GI17,** and **GI16** indicate that degradation predominantly proceeds through the **GI4** intermediate. The **GI4** predominantly undergoes degradation via the **RAF** mechanism. The most favorable site is C14, exhibiting a rate constant of $9.84x10^{11}$ M^{-1} s^{-1} and leading to the formation of product **GP3**, which accounts for 67.7% of the total product yield. This is followed by C2, with a rate constant of $3.89x10^{11}$ M^{-1} s^{-1}, resulting in product **GP1** at 26.7%. At the C8 position, the reaction proceeds with a rate constant of 6.89×10^{10} M^{-1} s^{-1},

yielding product **GP2** with a contribution of 4.7%. C3 position has a rate constant of $1.03x10^{10}$ M^{-1} s^{-1}, generating only 0.7% of the product. Reactions via the **FHT** mechanism also occur at **C19** and **C20** positions, but their contributions are minimal (0.1% each). Therefore, the main products of the second step are **GP1**, **GP2**, and **GP3**, corresponding to the **C2, C8,** and **C14** positions of the **GI4** transition state.

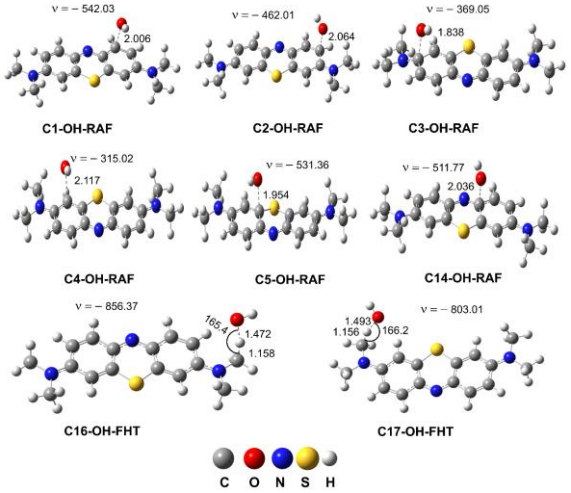

Figure 2. Structures of representative transition states *via* **FHT** and **RAF** nechanisms in the gas phase.

Based on the above analysis, it can be concluded that in the gas phase at 298.15 K, **MB** is primarily degraded by the HO• radical via the **RAF** mechanism at the C4 position, leading to the formation of three major products. The overall rate constants for steps 1 and 2 are $3.24x10^{10}$ M^{-1} s^{-1} and $1.45x10^{12}$ M^{-1} s^{-1}, respectively.

3.2.3. Effect of temperature on the degradation of MB in the gas phase

To investigate the effect of temperature on the degradation of **MB**, the rate constants for reactions at various positions of **MB** were calculated within the typical environmental temperature range (253 - 323 K, equivalent to -20°C to 50°C). The results are presented in **Figure 3**. As the gas-phase temperature increases, all rate constants associated with the **FHT** mechanism (k16, k17) decrease. In contrast, the rate constants corresponding to the **RAF** mechanism exhibit inconsistent trends: k1, k5, and k14 increase with temperature, while k2 and k4 decrease. Notably, k3 and k13 fluctuate irregularly. In the temperature range of 253 - 323 K, the overall rate constant for **MB** degradation tends to decrease, primarily due to the decline in k16, k17, k2, and k4, which correspond to the four reactive positions previously discussed in **Table 3**. Among all, k4 is the highest at every temperature (ranging from $1.81x10^{10}$ $M^{-1}s^{-1}$ to $6.63x10^{10}$ M^{-1} s^{-1}), indicating that the **RAF** mechanism at the C4 position is the most favorable. Therefore, the primary degradation products of **MB** are those formed via radical addition of HO• to **MB**, specifically **GP1, GP2**, and **GP3**.

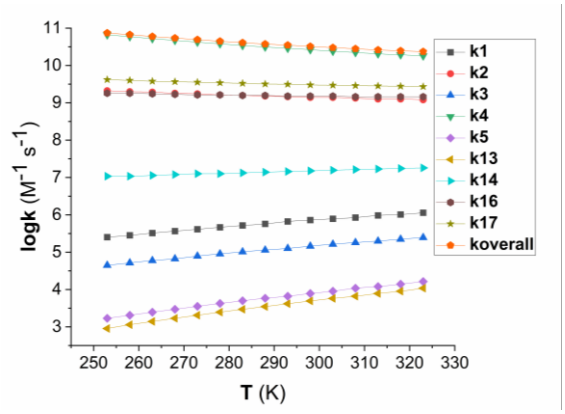

Figure 3. Temperature dependence of rate constants (log *k*) in the gas phase in the range of 253 - 323 K.

4. CONCLUSION

This study elucidates the mechanisms and kinetics associated with the degradation of **MB** by HO• radical in the gas phase, employing quantum chemical calculations. At a temperature of 298.15 K in the gas phase, **MB** undergoes degradation primarily through a radical adduct formation mechanism involving the HO• radical at the C4 position. This process yields three principal products, with the overall rate constants for steps 1 and 2 being 3.24×10^{10} $M^{-1}s^{-1}$ and 1.48×10^{12} $M^{-1}s^{-1}$, respectively. In the temperature range of 253 - 323 K, the overall rate constant for **MB** degradation tends to decrease.

Acknowledgments

REFERENCES

1. M.I. Din, R. Khalid, J. Najeeb, Z. Hussain. Fundamentals and photocatalysis of methylene blue dye using various nanocatalytic assemblies-a critical review, *Journal of Cleaner Production,* **2021**, *298*126567.
2. M. Rafatullah, O. Sulaiman, R. Hashim, A. Ahmad. Adsorption of methylene blue on low-cost adsorbents: a review, *Journal of*

Hazardous Materials, **2010**, *177*(1-3), 70-80.
3. M. Mohammed, A. Shitu, A. Ibrahim. Removal of methylene blue using low cost adsorbent: a review*, Research Journal of Chemical Sciences,* **2014**, *2231*606X.
4. Q.V. Vo, L.T.T. Thao, T.D. Manh, M. Van Bay, B.-T. Truong-Le, N.T. Hoa, A. Mechler. Reaction of methylene blue with OH radicals in the aqueous environment: mechanism, kinetics, products and risk assessment*, RSC Advances,* **2024**, *14*(37), 27265-27273.
5. M. J. Frisch, G. W. Trucks, H. B. Schlegel, G. E. Scuseria, M. A. Robb, J. R. Cheeseman, G. Scalmani, V. Barone, B. Mennucci, G. A. Petersson, H. Nakatsuji, M. Caricato, X. Li, H. P. Hratchian, A. F. Izmaylov, G.Z. J. Bloino, J. L. Sonnenberg, M. Hada, M. Ehara, K. Toyota, R. Fukuda, J. Hasegawa, M. Ishida, T. Nakajima, Y. Honda, O. Kitao, H. Nakai, T. Vreven, J. A. Montgomery, J.E.P. Jr., F. Ogliaro, M. Bearpark, J. J. Heyd, E. Brothers, K. N. Kudin, V. N. Staroverov, T. Keith, R. Kobayashi, J. Normand, K. Raghavachari, A. Rendell, J. C. Burant, S. S. Iyengar, J. Tomasi, M. Cossi, N. Rega, J. M. Millam, M. Klene, J. E. Knox, J. B. Cross, V. Bakken, C. Adamo, J. Jaramillo, R. Gomperts, R. E. Stratmann, O. Yazyev, A. J. Austin, R. Cammi, C. Pomelli, J. W. Ochterski, R. L. Martin, K. Morokuma, V. G. Zakrzewski, G. A. Voth, P. Salvador, J. J. Dannenberg, S. Dapprich, A. D. Daniels, O. Farkas, J. B. Foresman, J. V. Ortiz, J. Cioslowski, D. J. Fox, *Gaussian 16, Revision A.03*. 2016, Gaussian, Inc., Wallingford CT: Gaussian, Inc., Wallingford CT.
6. M. Carreon-Gonzalez, A. Vivier-Bunge, J.R. Alvarez-Idaboy. Thiophenols, Promising Scavengers of Peroxyl Radicals: Mechanisms and kinetics*, Journal of Computational Chemistry,* **2019**,
7. N. Mora-Diez, J.R. Alvarez-Idaboy, R.J. Boyd. A quantum chemical and TST study of the OH hydrogen-abstraction reaction from substituted aldehydes: FCHO and ClCHO*, Journal of Physical Chemistry A,* **2001**, *105*(39), 9034-9039.
8. A. Galano, J.R. Alvarez-Idaboy. Kinetics of radical-molecule reactions in aqueous solution: A benchmark study of the performance of density functional methods*, Journal of Computational Chemistry* **2014**, *35*(28), 2019-2026.
9. A. Galano, G. Mazzone, R. Alvarez-Diduk, T. Marino, J.R. Alvarez-Idaboy, N. Russo. Food antioxidants: chemical insights at the molecular level*, Annual Review of Food Science and Technology,* **2016**, *7*335-352.
10. M.E. Alberto, N. Russo, A. Grand, A. Galano. A physicochemical examination of the free radical scavenging activity of Trolox: mechanism, kinetics and influence of the environment*, Physical Chemistry Chemical Physics,* **2013**, *15*(13), 4642-4650.
11. M.G. EvansM. Polanyi. Some applications of the transition state method to the calculation of reaction velocities, especially in solution*, Transactions of the Faraday Society* **1935**, *31*875-894.
12. H. Eyring. The Activated Complex in Chemical Reactions*, The Journal of Chemical Physics,* **1935**, *3*(2), 107-115.
13. D.G. Truhlar, W.L. Hase, J.T. Hynes. Current Status of Transition-State Theory*, Journal of Physical Chemistry,* **1983**, *87*(15), 2664-2682.
14. T. Furuncuoglu, I. Ugur, I. Degirmenci, V. Aviyente. Role of chain transfer agents in free radical polymerization kinetics*, Macromolecules,* **2010**, *43*(4), 1823-1835.
15. E. Vélez, J. Quijano, R. Notario, E. Pabón, J. Murillo, J. Leal, E. Zapata, G. Alarcón. A computational study of stereospecifity in the thermal elimination reaction of menthyl benzoate in the gas phase*, Journal of Physical Organic Chemistry,* **2009**, *22*(10), 971-977.
16. E. Dzib, J.L. Cabellos, F. Ortíz-Chi, S. Pan, A. Galano, G. Merino. Eyringpy: A Program for Computing Rate Constants in the Gas Phase and in Solution*, International Journal of Quantum Chemistry,* **2019**, *119*(2), e25686.
17. E. Dzib, J. L. Cabellos, F. Ortiz-Chi, S. Pan, A. Galano, G. Merino. *Eyringpy 1.0.2,* **2018**, Cinvestav, Mérida, Yucatán.
18. C. Eckart. The penetration of a potential barrier by electrons*, Physical Review,* **1930**, *35*(11), 1303.
19. E. PollakP. Pechukas. Symmetry numbers, not statistical factors, should be used in absolute rate theory and in Broensted relations*, Journal of the American Chemical Society,* **1978**, *100*(10), 2984-2991.
20. A. Fernández-Ramos, B.A. Ellingson, R. Meana-Pañeda, J.M. Marques, D.G. Truhlar. Symmetry numbers and chemical reaction rates*, Theoretical Chemistry accounts,* **2007**, *118*(4), 813-826.
21. H.E. Marr, J.M. Stewart, M. Chiu. The crystal structure of methylene blue pentahydrate*, Acta Crystallographica Section B: Structural Crystallography and Crystal Chemistry,* **1973**, *29*(4), 847-853.